SUPPORTING INFORMATION for:

Composition Dependence of Ionic Conductivity in LiSiPO(N) Thin-Film Electrolytes for Solid-State Batteries

*Theodosios Famprikis[a,b,c], Jules Galipaud[b], Oliver Clemens[c,d], Brigitte Pecquenard[b *], and Frédéric Le Cras[a*]*

[a]Univ. Grenoble Alpes, CEA, LETI, F-38054 Grenoble, France

[b]CNRS, Université de Bordeaux, ICMCB and Bordeaux INP, F-33600 Pessac, France

[c]Institute of Materials Science, Materials Design by Synthesis, Technische Universität Darmstadt, 64287 Darmstadt, Germany

[d]Institute of Nanotechology, Karlsruhe Institute of Technology, Hermann-von-Helmholtz-Platz 1, 76344 Eggenstein-Leopoldshafen, Germany.

Corresponding Authors

frederic.lecras@cea.fr; brigitte.pecquenard@icmcb.cnrs.fr

Refinement of Target Material X-Ray Diffraction (XRD)

The full x-ray diffraction patterns of the target materials are presented in Figures S1-S3 along with their associated Rietveld refinement results. All analyses of diffraction data were performed by using the Rietveld method as implemented in TOPAS V5 (Bruker AXS). The microstructural parameters (crystallite size and strain broadening) were refined to adjust the peak shapes (crystallite size only for phases with minor quantities). A model using two fractions of $Li_{3+x}Si_xP_{1-x}O_4$ was used to model the small additional reflection asymmetry, and the lattice parameters given here are weighted by the relative phase fraction of each of those phases. This model can be interpreted as a small fluctuation of composition between different crystallites. Thermal displacement parameters were constrained to be the same for all of atoms of all phases to minimize quantification errors and to account for angular dependent intensity changes induced by absorption and surface roughness. No atomic positions were refined for the phases within the refinement.

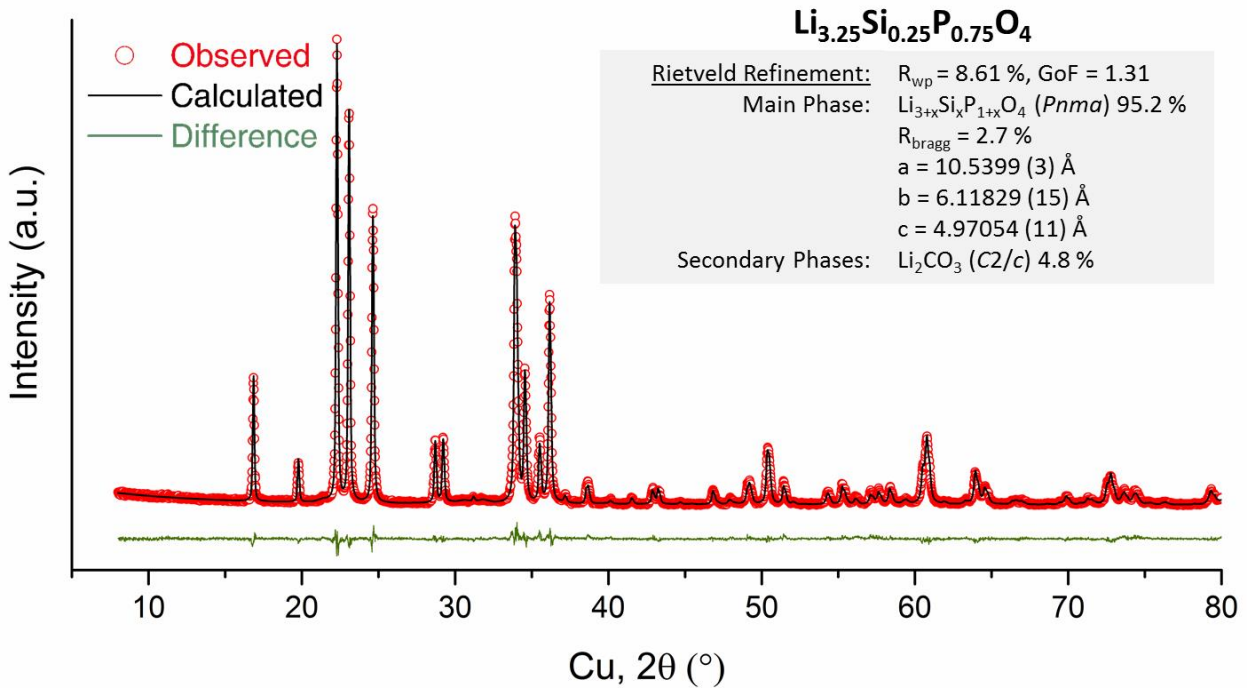

Figure S 1: Full x-ray powder diffraction pattern and Rietveld refinement of $Li_{3.25}Si_{0.25}P_{0.75}O_4$

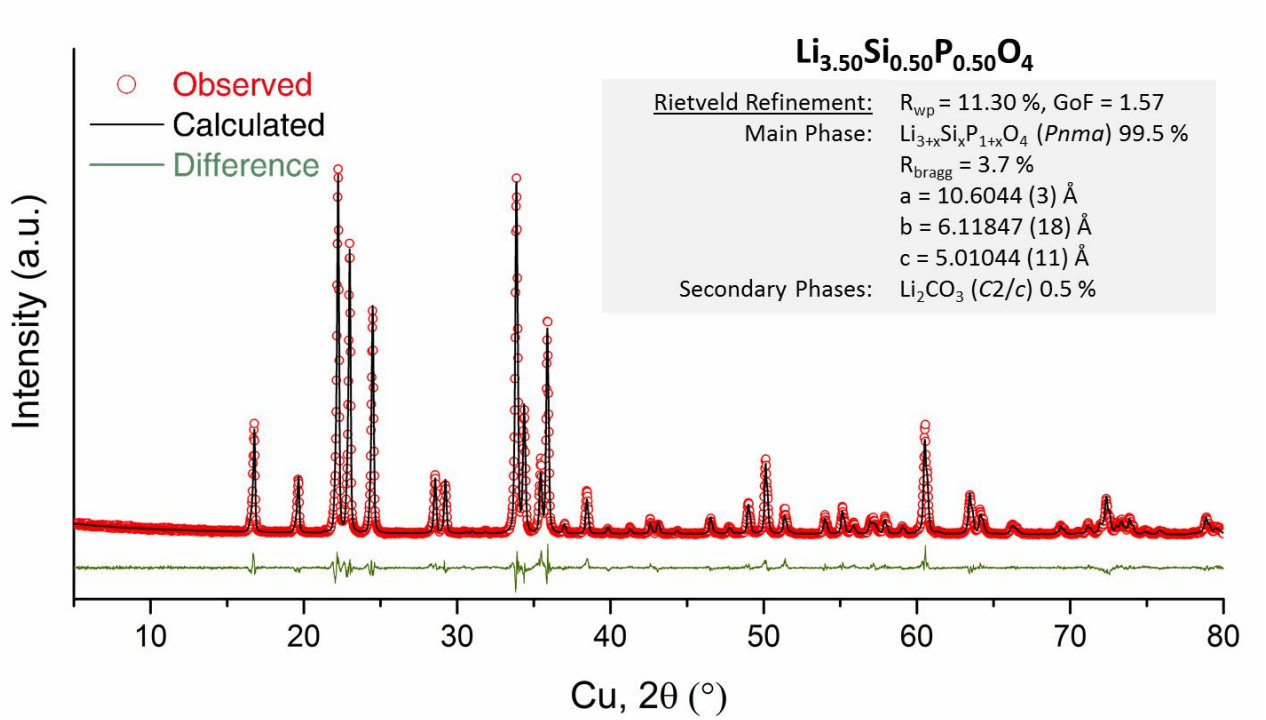

Figure S 2: Full x-ray powder diffraction pattern and Rietveld refinement of $Li_{3.50}Si_{0.50}P_{0.50}O_4$

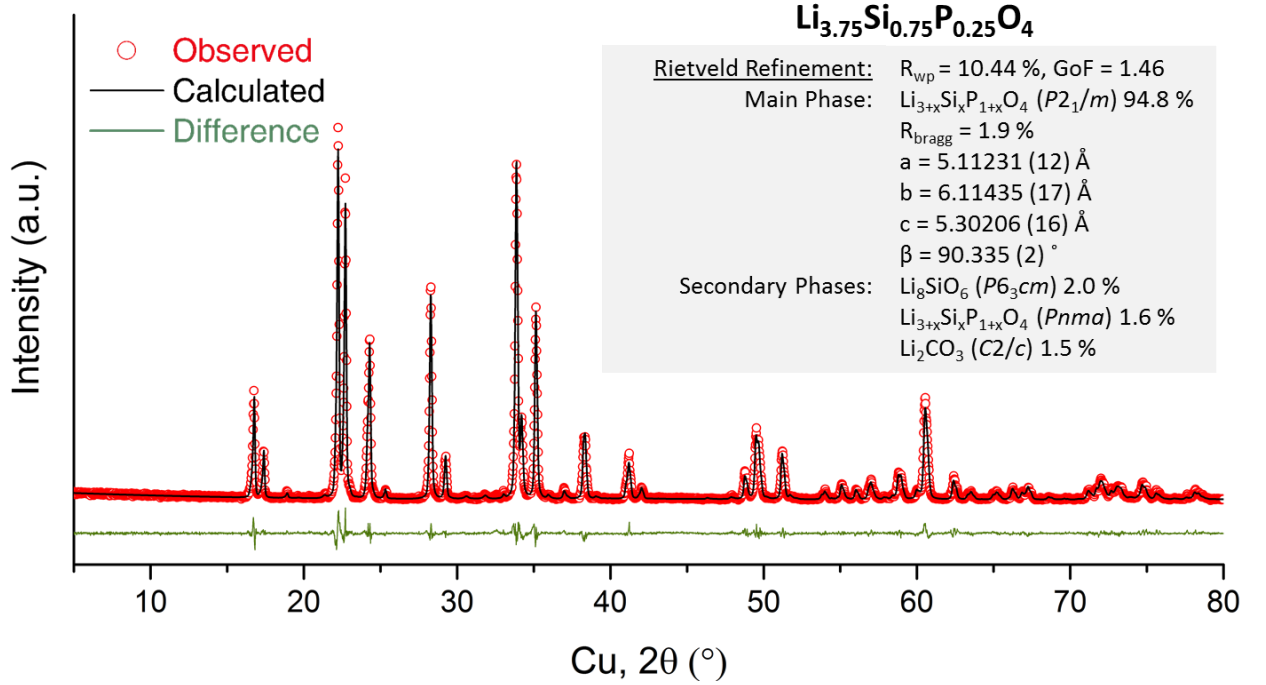

Figure S 3: Full x-ray powder diffraction pattern and Rietveld refinement of $Li_{3.75}Si_{0.75}P_{0.25}O_4$

Thin-film XRD

Diffractograms of selected, approximately 1 μm thick, thin films grown on silicon substrates were measured on a Bruker D8 Discover diffractometer equipped with a Göbel mirror. Collimation was ensured using a 0.05 mm slit on the primary beam and Soller slits on the diffracted beam. To increase the signal to noise ratio of the overall measurements, a Lynxeye 1D detector was used. Multiple measurements were performed at ambient conditions and successive short scans were used to monitor a possible evolution of the diffractograms due to reactivity with ambient air. Each scan was performed in the range 2°-60°, with a step of 0.05° and a step duration of 0.5 sec for a total duration of approximately 10 minutes. The diffractograms presented below represent the addition of 10 x 10-minute scans.

Only the reflections of the Si substrate are observable in all samples measured (highlighted in Figure S 4), attesting to the amorphous nature of the films. The substrate being a monocrystalline Si wafer, the intensity of these reflections is greatly influenced by the orientation of the sample with respect to the incident x-ray beam.

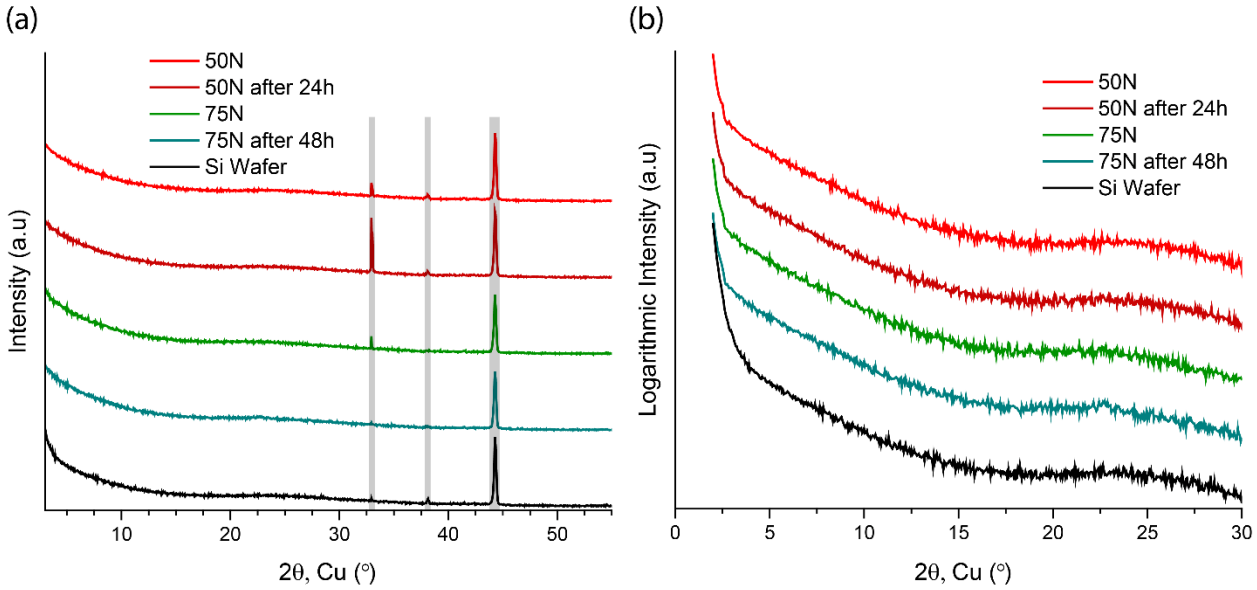

Figure S 4: X-ray diffractograms of the 50N and 75N thin films grown on Si substrates in (a) linear and (b) logarithmic intensity scales. Highlighted reflections originate from the silicon wafer substrate.

Electron-probe microanalysis (EPMA) and inductively coupled plasma optical emission spectroscopy (ICP-OES)

EPMA was performed on 10 spots and with three different acceleration voltages (5, 10 and 15 kV) for each thin-film sample. The relative atomic ratio of silicon, phosphorus, oxygen and nitrogen on the sample (as well as Ti and Al from the substrate) were determined by following the intensities of the Si Kα, P Kα, O Kα, N Kα, Ti Kα and Al Kα peaks, the positions of which were previously calibrated on pure silicon (Si), indium phosphide (InP), silicon dioxide (SiO_2), silicon nitride (Si_3N_4), metallic titanium (Ti) and metallic aluminium (Al) reference samples, respectively. The results were fitted using the LayerQuant module of the PeakSight software suite (CAMECA) using the thicknesses determined by profilometry and assuming a density of 2.4 g/cm^3 for the thin films. This fitting also allowed calculation of the lithium content in the films, which is not directly measurable by EPMA due to the low electronic density of Li.

In order to elucidate the lithium content directly, the LiSiPO(N) thin films of at least 1 µm, grown on approximately 3x2 cm^2 glass substrates were dissolved in a boiling acidic solution made by diluting 10ml of 34% HCl in 20 ml of deionized water. The solutions were then diluted and analyzed by ICP-OES using a Varian Inc. 720ES to determine their concentration in Li, P and Si. Given the accuracy of ICP-OES for determining the composition of metals, and especially alkali metals, these results are used to refine the compositions by combining the absolute wt% (x_i) of Li from ICP-OES [i] and the relative at% (y_i) among Si, P, O and N from EPMA. The interconversions were performed using the following equations where M_i is the atomic weight of element i, and M_T is the mean atomic weight of the LiSiPO(N) film, both in g/mol.

$$x_i = 1 - \sum_{j \neq i} x_j \qquad \text{S1}$$

$$x_i = \frac{y_i M_i}{M_T} \qquad \text{S2}$$

$$M_T = \sum_i y_i M_i \qquad \text{S3}$$

The resulting final normalized atomic compositions, combining the best accuracy of both techniques, are presented in Table 1 in the main text.

[i] The P and Si contents from ICP-OES were not used due to inconsistent results for the Si-rich samples arising from issues with sample digestion (SiO_2 is not soluble in HCl).

Electrochemical impedance spectroscopy (EIS) measurements

Through successive PVD depositions of metal and LiSiPON solid electrolyte through appropriate custom masks, the following samples were prepared in which a metal/LiSiPO(N)/metal cell is created for electrochemical impedance spectroscopy. The metal used was either gold or stainless steel and acted as both a blocking electrode and electrical contact, as shown in Figure S 5. The sample was transferred in a custom sample holder, sealed under argon, to the impedance analyzer for measurement.

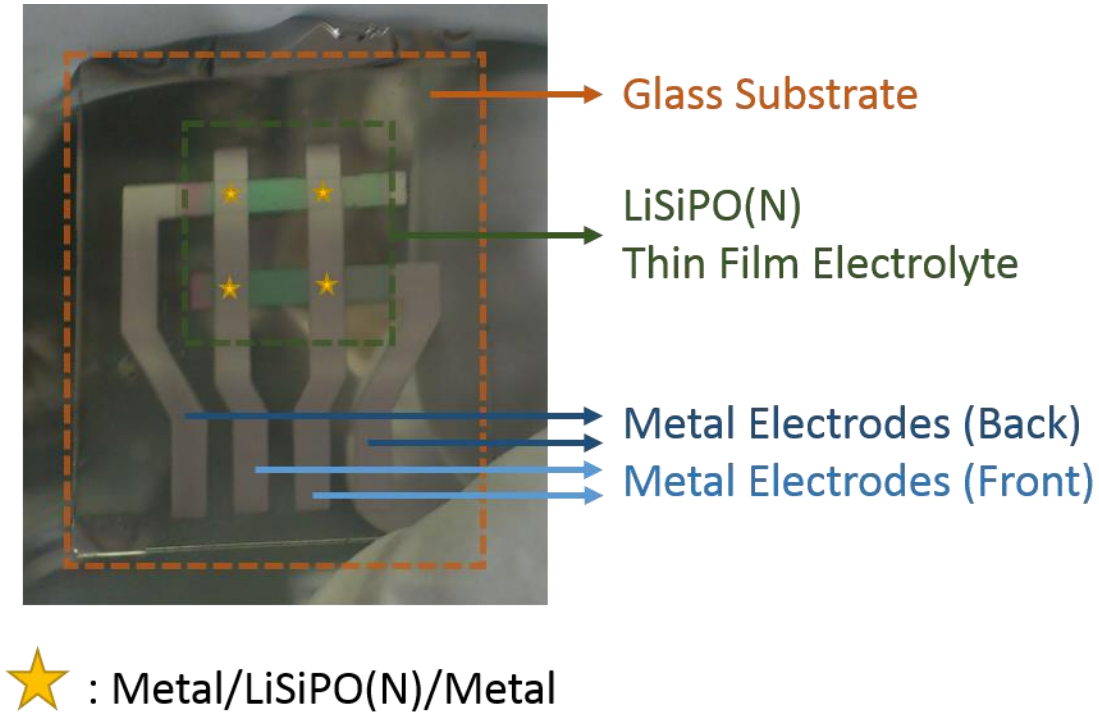

Figure S 5: Sample preparation for electrochemical impedance spectroscopy. The LiSiPO(N) thin film is deposited between metal electrodes creating four metal-electrolyte-metal structures for analysis.

Analysis of the EIS data

Characteristic impedance spectra of all samples at 30 °C are shown in Nyquist and modulus-Bode coordinates in Figure S6.

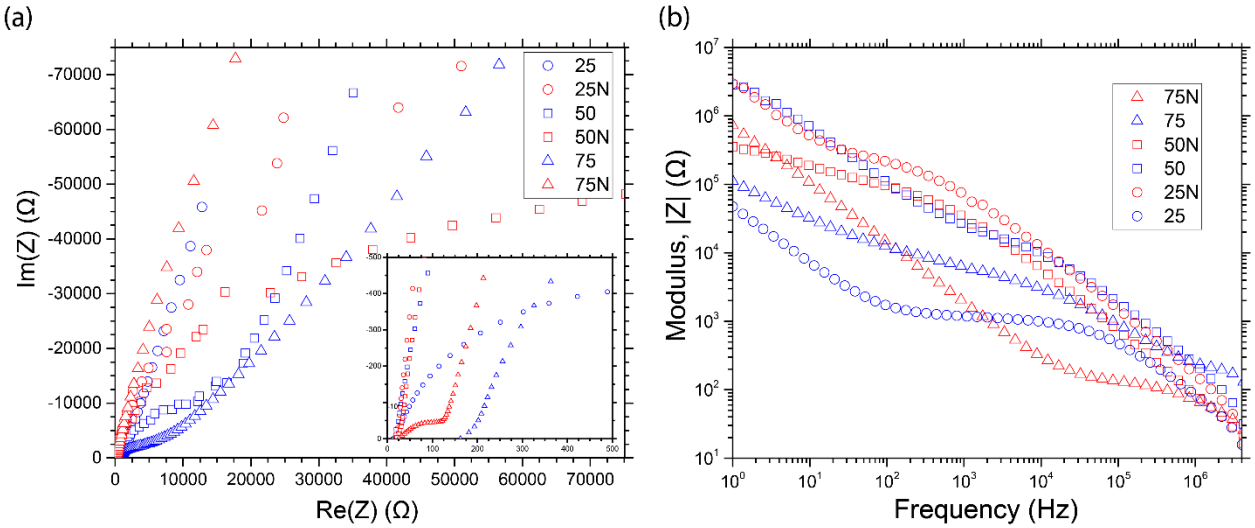

Figure S 6: (a) Nyquist and (b) modulus-Bode plots of the impedance spectra measured for all thin-film samples at 30 °C.

The impedance spectra were modelled using the equivalent circuit shown in Figure S 7 using the commercial software ZView 2. The resistor, R_{wiring}, and constant phase element, CPE_{block}, are used to represent the electrical resistance and capacitance of the ionically-blocking metal electrodes at high and low frequency regimes, respectively. The resistor R_{SE} and constant phase element CPE_{SE} in parallel are used to model the Li^+ ionic diffusion in the solid electrolyte.

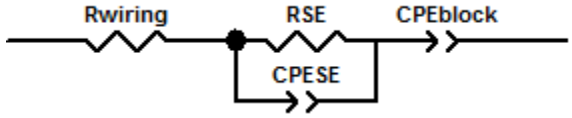

Figure S 7: Equivalent circuit model utilized to analyze the electrochemical impedance spectra.

Initial values for the parameters of the different elements are obtained through examination of the Nyquist and Bode plots of the impedance spectra (Figure S 8 and Figure S 9). Specifically, by determining the x-intercept and minimum of the derivative of the phase angle (i.e. dθ/df) one can determine the characteristic cutoff and apex frequencies, f_{cutoff} and f_{apex}, respectively. The real impedance at f_{cutoff} corresponds approximately to the sum of resistances $R_{wiring}+R_{SE}$. f_{apex} can then serve to derive the capacitance of CPE_{SE} through Eq. S4:

$$f_{apex} = \frac{1}{2\pi RC} \qquad \text{S4}$$

The capacitance C_{SE} is then related to the CPE parameters, Y_o and α, by Eq. S5:

$$C = Y_0^{\frac{1}{\alpha}} R^{\frac{1-\alpha}{\alpha}} \qquad \text{S5}$$

Once the spectra have been fitted, the intrinsic conductivity (σ) and relative permittivity (ε) of the thin films can be calculated from the extracted R_{SE} and C_{SE} by Eqs. S6 and S7:

$$\sigma = \frac{d}{RA} \quad \text{S6}$$

$$\varepsilon = \frac{Cd}{A\varepsilon_0} \quad \text{S7}$$

where d and A are the thickness of the thin film and the area of the metal electrodes through which impedance is analyzed, respectively (see Figure S 5). ε_o is the permittivity of free space equal to $8.85 \cdot 10^{-12}$ F/m.

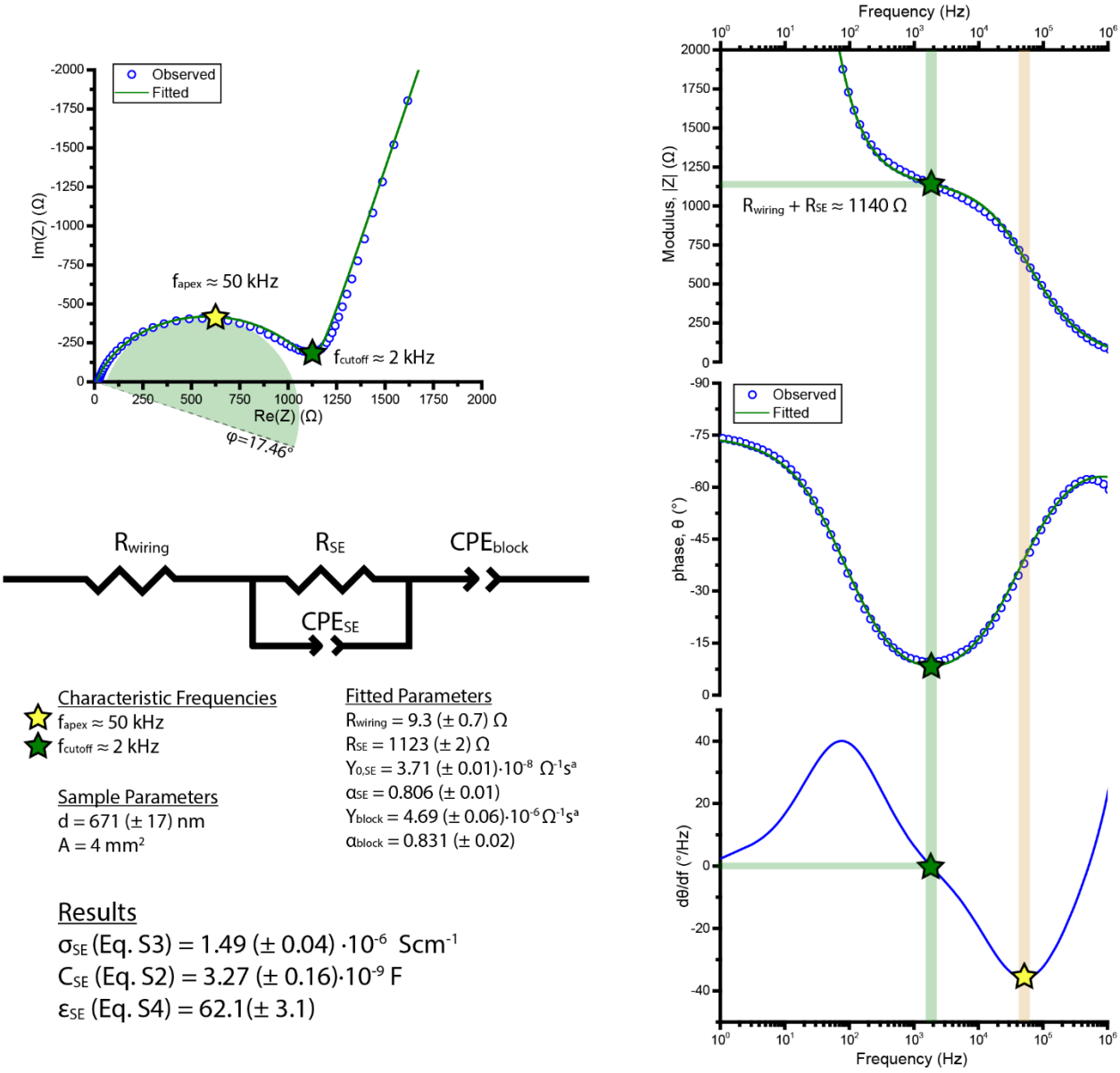

Figure S 8: Nyquist and Bode plots of the impedance spectra collected from the 25 sample at 30 °C, deposited from the $Li_{3.25}Si_{0.25}P_{0.75}O_4$ target under Ar flow. The characteristic frequencies f_{apex} and f_{cutoff} are determined from the derivative of the phase angle wrt. frequency and are utilized to provide physical initial values for the fit. The parameters utilized for the fit and their associated errors are presented.

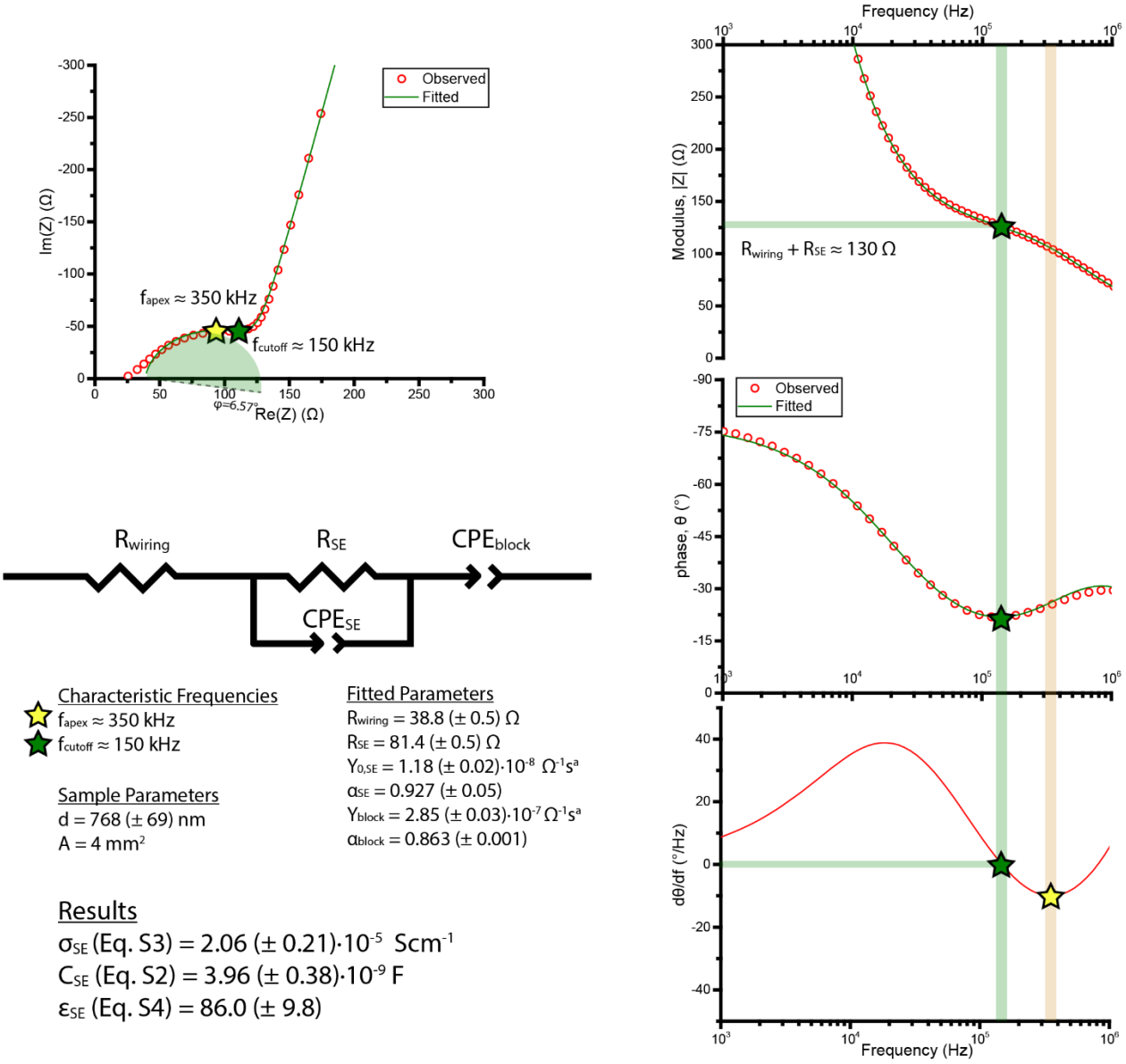

Figure S 9: Nyquist and Bode plots of the impedance spectra collected from the 75N sample at 30 °C, deposited from the $Li_{3.75}Si_{0.75}P_{0.25}O_4$ target under N_2 flow. The characteristic frequencies f_{apex} and f_{cutoff} are determined from the derivative of the phase angle wrt. Frequency and are utilized to provide physical initial values for the fit. The parameters utilized for the fit and their associated errors are presented.

The capacitance, C, of an R-CPE loop is typically used to qualitatively identify the origin of the conduction process observed. Irvine, Sinclair and West suggested the following capacitance regimes for the various phenomena observable through impedance spectroscopy on **macroscopic samples, with an aspect ratio of diameter d to area A, d/A = 1 cm^{-1}** [1]. In order to place our results in this framework we convert to the dimensionless relative permittivity, ε, through Eq. S7 to account for the thin-film geometry, as listed in Table S 1.

Table S 1: Associations of observable capacitance and electrochemical phenomena as proposed in ref. 1

Phenomenon Responsible	Macroscopic (d/A= 100 m^{-1}) Capacitance [F]	Relative permittivity	Thin-Film (d/A=0.1 m^{-1}) Capacitance [F]
bulk	10^{-12}	~10	~10^{-9}
minor, second phase	10^{-11}	~100	~10^{-8}
grain boundary	10^{-11}-10^{-8}	~10^{2}-10^{5}	~10^{-8}-10^{-5}
bulk ferroelectric	10^{-10}-10^{-9}	~10^{3}-10^{4}	~10^{-7}-10^{-6}

All thin-film samples tested exhibited a relative permittivity in the range 50-100 which is consistent with Li-ion transport in the bulk (Figure S 10).

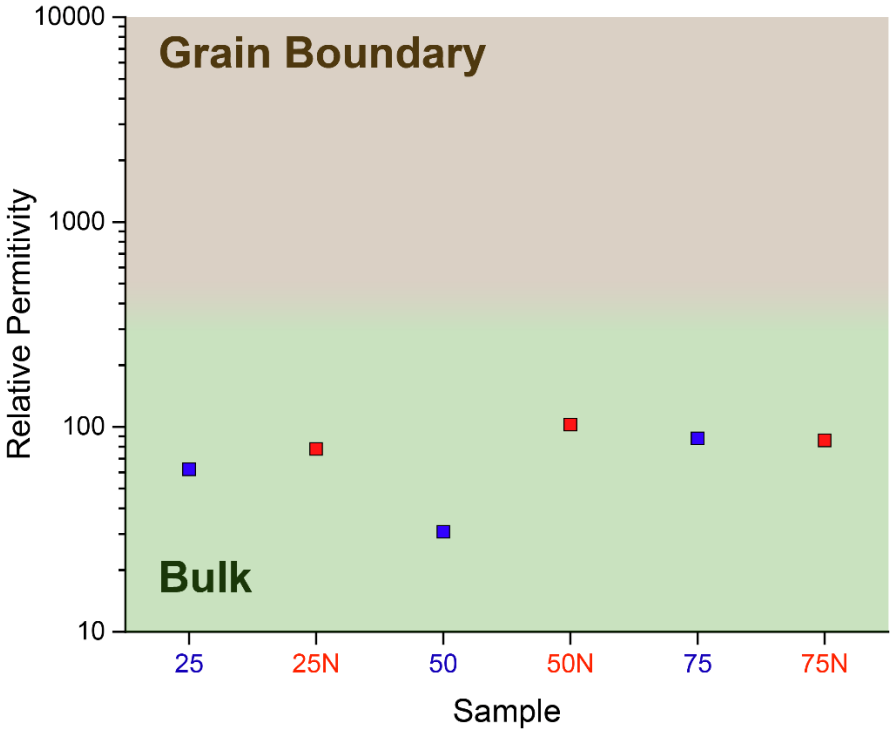

Figure S 10: Relative permittivities of the LiSiPO(N) thin-film samples as extracted from electrochemical impedance spectroscopy. The values correspond to ion conduction in the bulk.

The characteristic frequencies observed in the impedance spectra of the LiSiPO(N) thin-film samples exhibited a wide variance (Table S 2) and correlate qualitatively with the observed conductivity (Figure S 11).

Table S 2: Observed characteristic frequencies observed on the LiSiPON thin-film samples at 30 °C.

Sample	25	25N	50	50N	75	75N
Apex Frequency (Hz)	50000	3500	13000	500	15000	350000
Cutoff Frequency (Hz)	2000	75	2000	15	500	150000

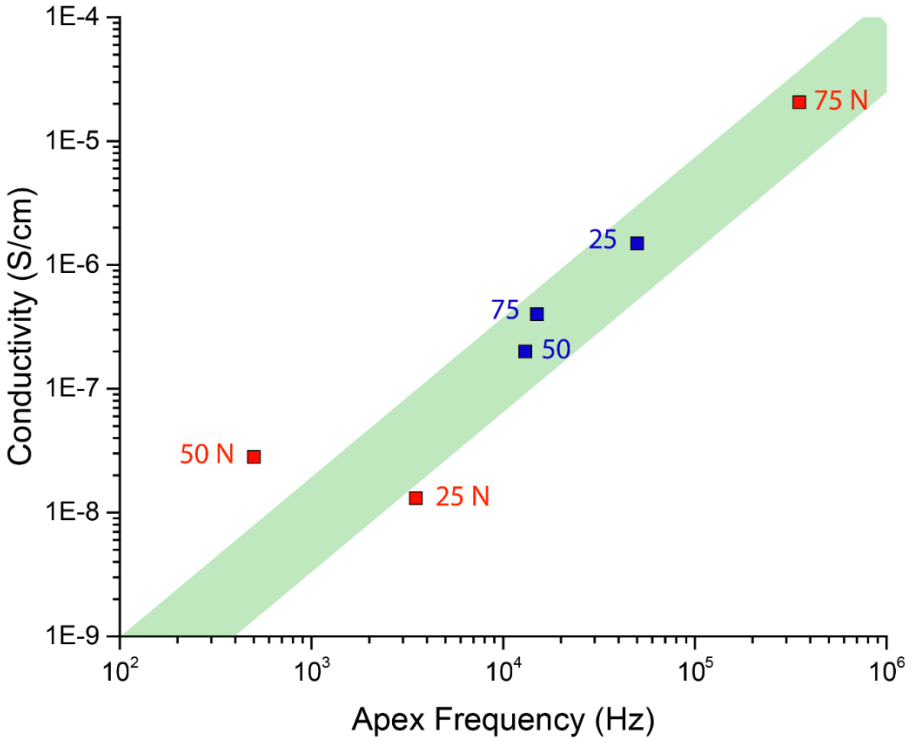

Figure S 11: Qualitative correlation between apex frequency and conductivity for the LiSIPON thin films studied.

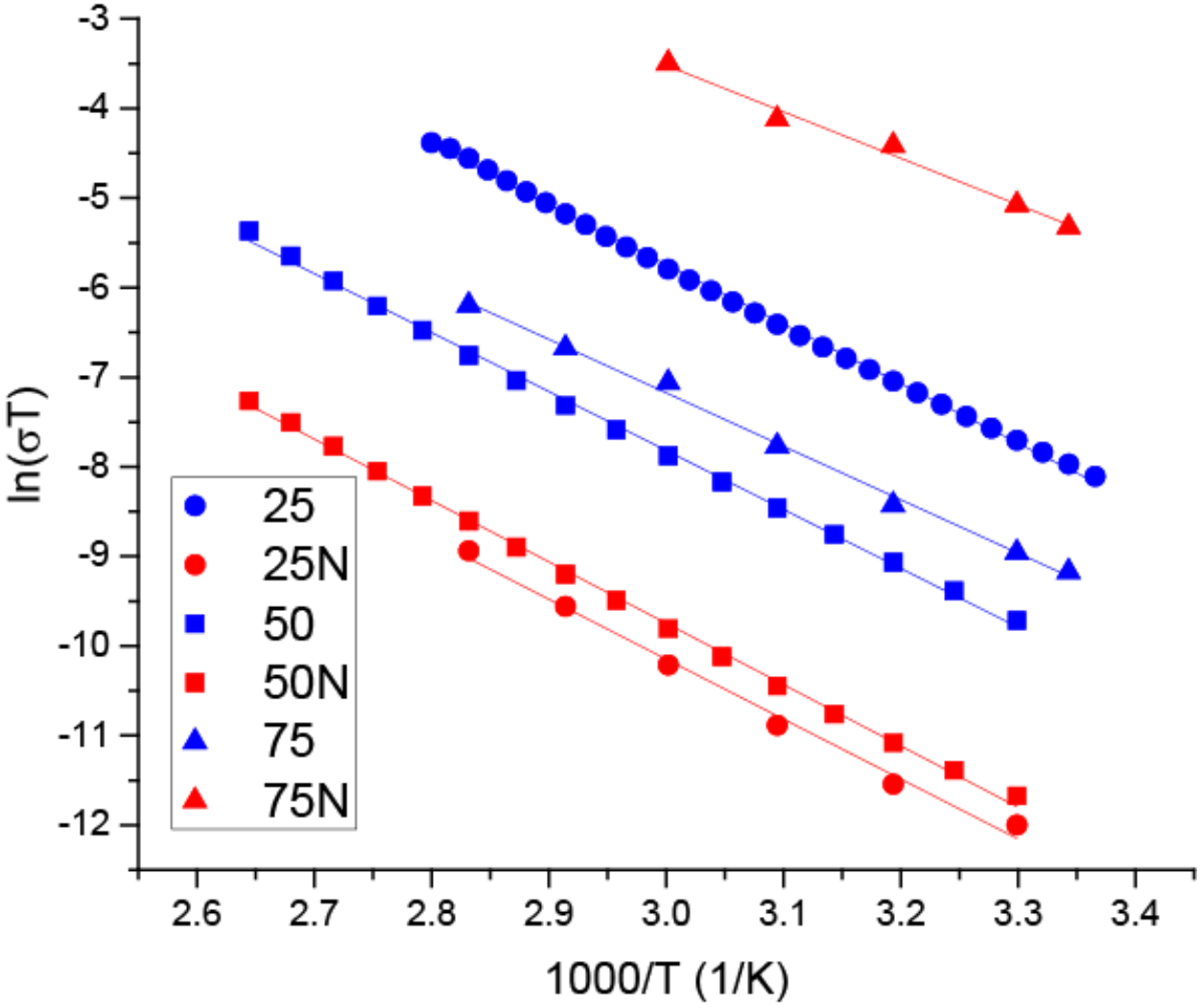

Figure S 12: Arrhenius plot of the conductivity values derived from EIS for LiSiPO(N) thin film electrolytes and associated linear fits used to derive the activation energies reported in Table 1 of the main text.

Literature Composition and Conductivity Values of LiSiPO Thin-Film Electrolytes

Table S 3: Values of Li and Si molar composition, ionic conductivity and activation energy for conduction of LiSiPO thin films in published literature. Hyphens (-) indicate that a value was not reported.

Internal Sample Name	Li/(Si+P) (at.)	Si/(Si+P) (at.)	Conductivity @RT (S/cm)	Activation Energy (eV)	Reference
	-	0.55	1.67E-7	0.79	
3:6:1 + Li_3PO_4	-	0.43	4.2E-8	0.8	
	-	0.4	4E-8	0.81	
3:4:1	-	0.5	2E-9	0.88	
		0.52	4E-10	-	
Sectored-1⁺	-	0.68	1E-8	0.92	2
	-	0.56	1E-9	0.93	
Sectored-2⁺⁺	-	0.37	8E-10	0.95	
	-	0.32	4.9E-8	0.95	
3:5:0.05 + Li_2O	-	0.67	4.2E-8	0.77	
	-	0.64	3E-10	1.04	
1:1 + Li_2O (Ar only)	2.84615	0.5	1.9E-7	0.65	
1:1 + Li_2O (Ar/O_2)	2.125	0.4375	5E-7	0.6	3
1:1 HP	1.43902	0.5122	1.6E-7	0.61	
1:1 HP	1.17391	0.5	9E-8	0.62	
1:1 sintered	0.47059	0.54412	6E-10	0.74	
1:1 sintered	0.19048	0.5	1.2E-16	1.16	
$Li_{3.6}Si_{0.6}P_{0.4}O_4$	-	0.6 [target]	5E-6	0.52	4
64B	2.5098	0.45098	3.84E-7	-	
67B	2.93333	0.51111	1.88E-7	-	
52B	2.19608	0.72549	6.7E-8	-	5
108B	0.60976	0.82927	3.4E-9	-	
79B	0.78947	0.84211	1.5E-9	-	
98B	1.01299	0.84416	3.4E-9	-	

	2.7037	0	7E-8	0.64	
Li_2O-P_2O_5	2.22581	0	5E-8	0.63	
	2.0303	0	3E-9	0.84	[6]
Li_3PO_4	2.8	0	7E-8	0.67	
Li_3PO_4-SiO_2	2	0.33333	3.9E-7	0.61	
Li_3PO_4	2.7	0	7E-8	0.68	[7]
Li_3PO_4 + Li_4SiO_4	3.564	0.1919	2E-7	0.57	
50:50	3.5 [target]	.5	1.6E-6	1.6E-6	
Li_3PO_4	3 [target]	0	5.1E-7	5.1E-7	[8] [PLD]
Li_4SiO_4	4 [target]	1	1.2E-8	1.2E-8	
25	0.94	0.30	1.49E-6	0.57	
50	0.97	0.59	2.00E-7	0.56	This Work
75	2.40	0.88	4.09E-7	0.51	

We underline that the LiSiPO thin films reported above have been prepared by various process parameters (RF-power, process gas, pressure) and most notably utilizing different targets. As such the values are not strictly comparable but rather indicative of the general trends. For more details the reader is directed to the primary references.

Literature Composition and Conductivity Values of LiSiPON Thin-Film Electrolytes

Table S 4: Values of Li and Si molar composition, ionic conductivity and activation energy for conduction of LiSiPON thin films in published literature. Hyphens (-) indicate that a value was not reported.

Internal Sample Name	Li/(Si+P) (at.)	Si/(Si+P) (at.)	Conductivity @RT (S/cm)	Activation Energy (eV)	Reference
1#	-	0.83	6.8E-6	-	
2#	-	0.75	-	-	[9]
3#	-	0.68	-	-	
-	0.96	0.56	4.83E-6	-	[10]
a	1.80	0.22	2.88E-6	-	
b	1.91	0.24	8.61E-6	-	
c	1.86	0.31	1.04E-5	-	[11]
d	1.77	NA	3.45E-6	-	
e	1.58	0.25	2.21E-6	-	
f	1.90	0.27	1.43E-6	-	
A	1.92	0.17	5.65E-6	0.50	
B	1.48	0.22	8.86E-6	0.49	[12]
C	2.12	0.26	1.00E-5	0.49	
D	2.00	0.31	1.24E-5	0.48	
A	3.61	0.08	5.4E-6	0.47	
B	3.01	0.28	6.6E-6	0.45	[13]
C	3.22	0.48	9.7E-6	0.41	
25N	0.54	0.26	1.31E-8	0.58	
50N	0.56	0.56	2.81E-8	0.58	This Work
75N	1.35	0.79	2.06E-5	0.45	

We underline that the LiSiPON thin films reported above have been prepared by various process parameters (RF-power, process gas, pressure) and most notably utilizing different targets. As such the values are not strictly comparable but rather indicative of the general trends. For more details the reader is directed to the primary references.

Analysis of the Target Residue

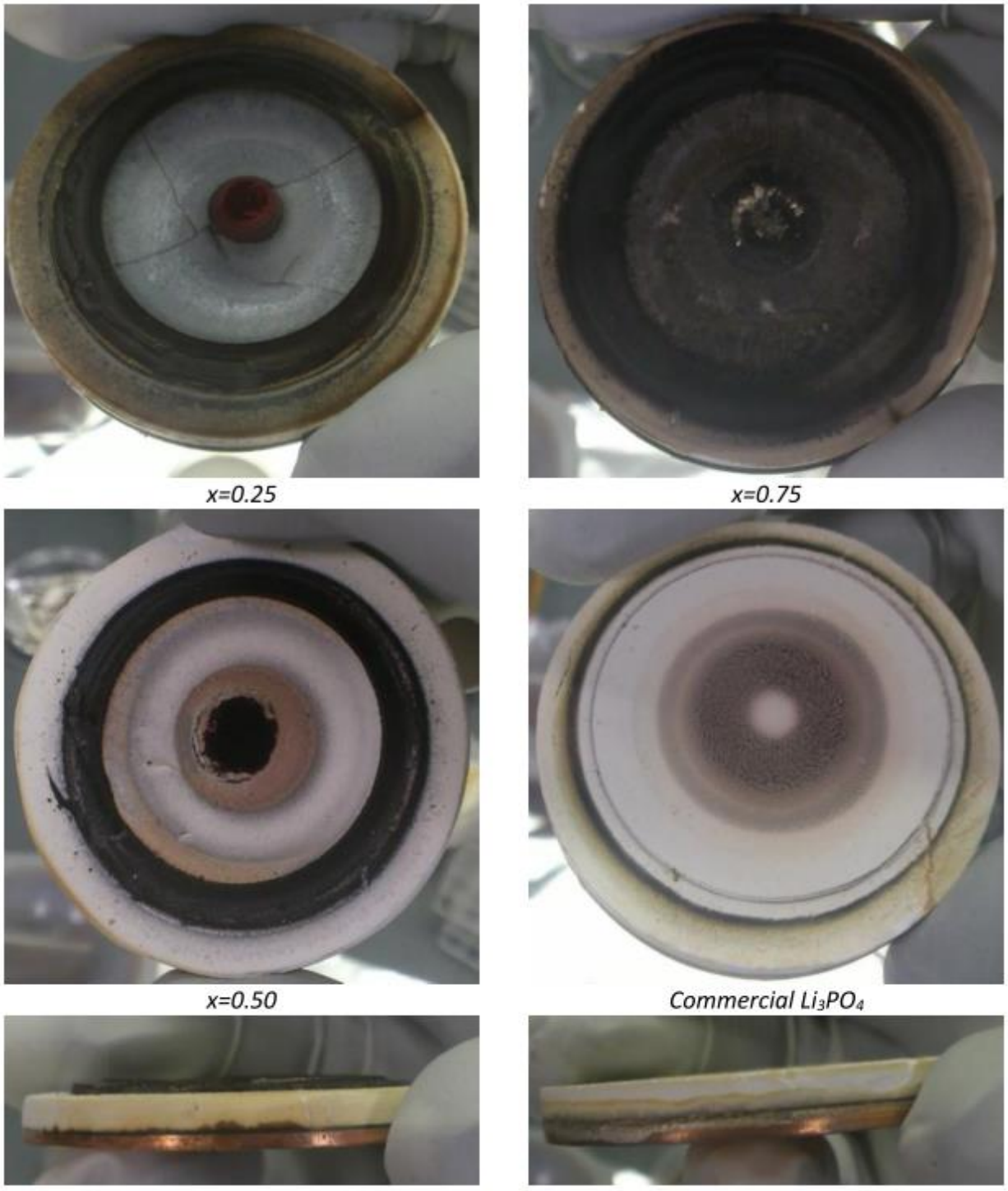

Figure S 13: Photographs of the $Li_{3+x}Si_xP_{1-x}O_4$ targets used after depositions.

The crystalline composition of the black material on the surface of the targets was identified by PXRD as predominantly Li_2O in all cases. The Li_2O peaks exhibit an anisotropy not observed for those of Li_3P. This anisotropy was refined with a distribution of three phases (giving rise to the three lattice parameters listed in Figure S 14). This can be interpreted as lattice strain or partial peroxide character ($Li_{2-x}O$).

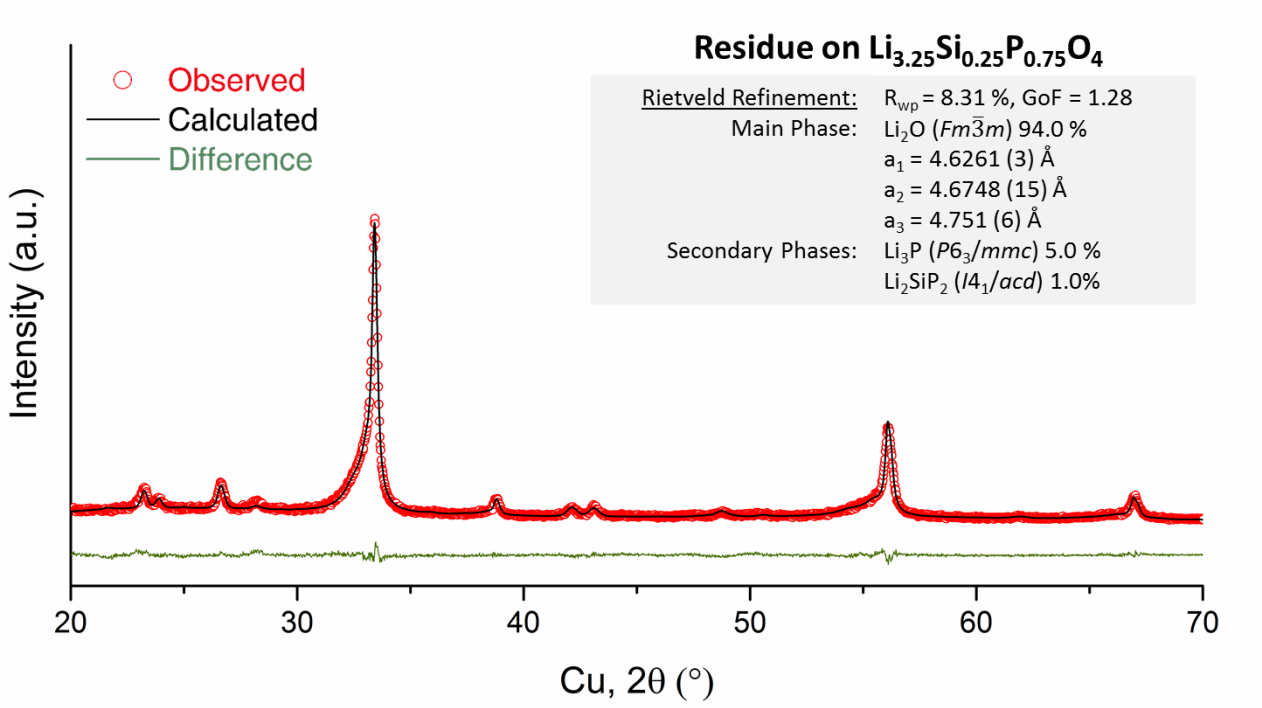

Figure S 14: Rietveld refinements of the black residue on the $Li_{3.25}Si_{0.25}P_{0.75}O_4$ target after deposition.

The analogous diffractograms from the other two targets (x = 0.50 and x = 0.75) exhibited similar features with the addition of unidentified peaks which likely correspond to Si-containing decomposition products.

Preliminary Cyclic Voltammetry Measurements

The electrochemical stability of the LiSiPO(N) thin films against Li^+ was preliminarily probed in Li | LP100 | LiSiPO(N) | Ti coin cells. The LiSiPO(N) thin films (~1µm) were deposited on 100 µm titanium foil cut into 16 mm diameter disks. The coin cell stack consisted of the coated titanium disks, a 25 µm thick Celguard® separator, a 220 µm thick Viledon® separator, 200 µl of LP100 electrolyte (1 M of $LiPF_6$ in a 1:1:3 mixture of ethylene carbonate, propylene carbonate and dimethyl carbonate, respectively) and a 125 µm disk of lithium metal pressed unto a disk of stainless steel. The samples were analyzed at sweep rates of either 0.1 mV/s (25, 25N, 75 and 75N films) or 0.01 mV/s (50 and 50N films) for 5 or 2 cycles, respectively, using a Bio-Logic VMP3 Potentiostat and the data was collected with the EC-Lab software.

All samples examined by cyclic voltammetry showed similar behavior to the control samples (constructed with bare titanium cathodes). Figure S 15 presents the first sweep (from open circuit voltage to 0 vs Li/Li^+) and as such would contain evidence of any electrochemical reaction. A peak at around 1.4 V vs. Li/Li^+ can be seen for the control sample which can be attributed to the reduction of a surface oxide layer on the Ti substrate. A reversible peak around 0.5 V can be seen which can be attributed to the reduction and oxidation of a component in the steel coin cell casing (e. g. chromium oxide passivation layer). After the first sweep, the samples retained a constant profile, as can be seen in the inset of Figure S 15 with the superposition of the 5 cycles of the 25N sample. The absence of unique peaks, even at the extremely low sweep rate of 0.01 mV/sec, down to 0 vs Li/Li^+, indicates the excellent cathodic stability of the LiSiPO(N) films at voltages which are relevant for microbattery applications. Note that the thin film electrolytes were not put in direct contact with lithium; i.e. this does not prove *chemical* stability against in lithium, which still remains to be tested.

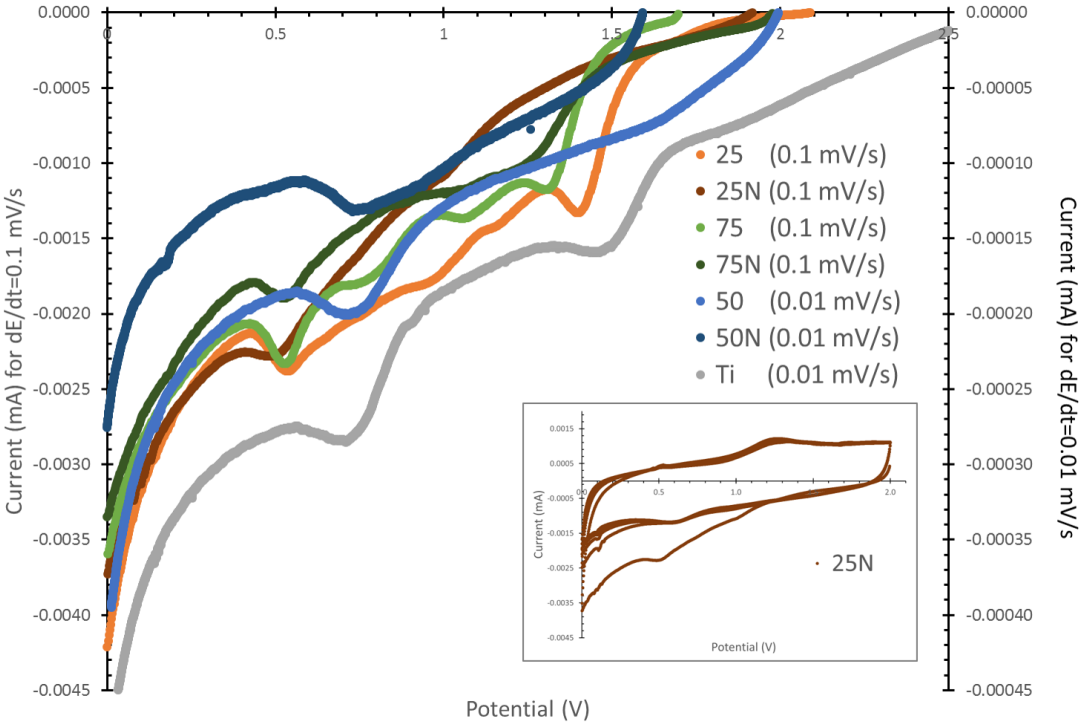

Figure S 15: Results of the first cycle of cyclic voltammetry on the LiSiPO(N)/LP100/Li cells All samples show the same peaks as the Ti control (in gray) indicating inertness under reducing conditions.

REFERENCES

(1) Irvine, J. T. S.; Sinclair, D. C.; West, A. R. Electroceramics: Characterization by Impedance Spectroscopy. *Adv. Mater.* **1990**, *2* (3), 132–138.

(2) Bates, J. B.; Dudney, N. J.; Chu, Y. T.; Mazumdar, P. Properties of Electrolyte and Electrode Films Prepared by RF and DC Magnetron Sputtering. *MRS Proc.* **1988**, *135*, 143.

(3) Bates, J. B.; Dudney, N. J.; Sales, B. C.; Robertson, J. D.; Zuhr, R. A.; Gruzalski, G. R.; Luck, C. F. Thin Film Amorphous Electrolytes: The Li_2O-SiO_2-P_2O_5 System. *MRS Proc.* **1990**, *210*, 569.

(4) Kanehori, K.; Matsumoto, K.; Miyauchi, K.; Kudo, T. Thin Film Solid Electrolyte and Its Application to Secondary Lithium Cell. *Solid State Ionics* **1983**, *9–10* (2), 1445–1448.

(5) Robertson, J. D.; Bates, J. B.; Dudney, N. J.; Zuhr, R. A. Ion Beam Analysis of Lithium-Ion Conducting Amorphous Electrolyte Films. *Nucl. Instruments Methods Phys. Res. Sect. B Beam Interact. with Mater. Atoms* **1991**, *56–57* (PART 2), 722–725.

(6) Bates, J. B.; Dudney, N. J.; Gruzalski, G. R.; Zuhr, R. A.; Choudhury, A.; Luck, C. F.; Robertson, J. D. Electrical Properties of Amorphous Lithium Electrolyte Thin Films. *Solid State Ionics* **1992**, *53–56*, 647–654.

(7) Bates, J. B.; Dudney, N. J.; Gruzalski, G. R.; Zuhr, R. A.; Choudhury, A.; Luck, C. F.; Robertson, J. D. Fabrication and Characterization of Amorphous Lithium Electrolyte Thin Films and Rechargeable Thin-Film Batteries. *J. Power Sources* **1993**, *43* (1–3), 103–110.

(8) Sakurai, Y.; Sakuda, A.; Hayashi, A.; Tatsumisago, M. Preparation of Amorphous Li_4SiO_4–Li_3PO_4 Thin Films by Pulsed Laser Deposition for All-Solid-State Lithium Secondary Batteries. *Solid State Ionics* **2011**, *182* (1), 59–63.

(9) Li, G. Synthesis on Microstructures and Properties of LiSiPON Solid State Electrolyte Thin Films. *J. Tianjin Norm. Univ.* **2013**, *33* (4), 16–19.

(10) Shen, W. Preparation and Characterization of Solid State Thin Film LiSiPON Electrolyte. *Chinese J. Power Sources* **2006**, *30* (3), 179–182.

(11) Xing, G. Fabrication and Electrochemical Properties Study of LiSiPON Electrolyte Films. *J. Guangdong Non-ferrous Met.* **2005**, *15* (2, 3), 462–466.

(12) Lee, S.-J.; Bae, J.-H.; Lee, H.-W.; Baik, H.-K.; Lee, S.-M. Electrical Conductivity in Li–Si–P–O–N Oxynitride Thin-Films. *J. Power Sources* **2003**, *123* (1), 61–64.

(13) Su, Y.; Falgenhauer, J.; Leichtweiß, T.; Geiß, M.; Lupó, C.; Polity, A.; Zhou, S.; Obel, J.; Schlettwein, D.; Janek, J.; Meyer, B. K. Electrochemical Properties and Optical Transmission of High Li + Conducting LiSiPON Electrolyte Films. *Phys. status solidi* **2017**, *254* (2), 1600088.